Available online at www.sciencedirect.com
SCIENCE DIRECT
Journal of Catalysis 236 (2005) 304–312
JOURNAL OF CATALYSIS
www.elsevier.com/locate/jcat

Involvement of active sites of promoted vanadyl pyrophosphate in selective oxidation of propane

Shinji Ieda, Satit Phiyanalinmat, Shin-ichi Komai, Tadashi Hattori, Atsushi Satsuma *

Department of Applied Chemistry, Graduate School of Engineering, Nagoya University, Furo-cho, Chikusa-ku, Nagoya 464-8603, Japan

Received 30 May 2005; revised 30 September 2005; accepted 7 October 2005

Available online 10 November 2005

Abstract

Involvement of active sites in the selective oxidation of propane was investigated using $(VO)_2P_2O_7$ catalysts promoted by Sb, Ti, Zr, Hf, Cu, and Ce. Based on X-ray diffraction patterns, infrared spectra, and Raman spectra, the formation of a $(VO)_2P_2O_7$ phase was confirmed for all of the promoted catalysts; no other phases were detected. After the addition of Sb, Ti, and Zr, the selectivity to acrylic acid increased, whereas Cu-, Ce-, and Hf-promoted catalysts showed lower selectivity than pure $(VO)_2P_2O_7$. The effect of promoters on the activity and selectivity for the propane oxidation was investigated on the basis of the nature of surface active sites. The surface V=O species, evaluated by the nitric oxide–ammonia rectangular pulse technique, decreased with the addition of the promoters. A proportional correlation between the number of surface V=O species and reaction rate of propane clarified that the surface V=O species is the controlling factor for the catalytic activity of propane oxidation. In the case of Sb-, Ti-, and Zr-promoted catalysts, the selectivity to acrylic acid increased significantly. The selectivity was compared with the number and strength of Brønsted and Lewis acid sites estimated from dimethylpyridine temperature-programmed desorption. A good correlation was observed between the selectivity to acrylic acid and the surface concentration of Lewis acid sites. It was experimentally demonstrated that Lewis acid sites represent the key factor in selective oxidation.

Keywords: Selective oxidation of propane; Vanadyl pyrophosphate; Effect of promoters; Solid Lewis acid; Surface V=O species

1. Introduction

Selective oxidation of lower alkane by molecular oxygen is of great interest in the catalysis research [1]. In particular, the selective oxidation of propane to acrylic acid using molecular oxygen as an oxidant is currently attracting much industrial and scientific attention [2–21]. Various catalysts have been reported to be active and selective for propane oxidation; these can be classified as (a) Mo-based mixed-oxide catalysts, such as Mo–V–Nb–Te mixed oxide, [2–9], Bi–Mo-based oxides [10,11], and Ag–Mo–P mixed oxide [12]; (b) heteropoly acid-based catalysts [13–16]; and (c) vanadyl phosphate-based catalysts [17–21]. Among these series of catalysts, Mo–V–Te–Nb mixed oxide is currently the most widely investigated, and a voluminous literature is available in both patents and scientific papers.

As for the Mo–V-based mixed-oxide catalysts, most of the reports to date have focused on the roles of the various components and the formation of a specific crystal phase. It is generally accepted that the catalytic performance of Mo–V–Te–Nb mixed oxide depends strongly on the crystal phase [22–27]. Tsuji and Koyasu identified an orthorhombic phase (phase *i*) and hexagonal phase (phase *k*) and noted that the former demonstrates higher catalytic performance in the selective oxidation of propane [22]. Katou et al. prepared a new orthorhombic Mo–V–O catalyst by hydrothermal synthesis and clarified the role of each element in Mo–V–Te–Nb oxide catalysts [25].

Although the effect of the bulk structure on catalytic performance has been well investigated, few papers have reported the roles of catalyst surface and surface functional species. Although the redox activity of the surface sites and the importance of Lewis acid sites have been pointed out, the roles of these sites have not been well investigated experimentally. The relationship between surface structure and catalytic performance

* Corresponding author. Fax: +81 52 789 3193.
E-mail address: satsuma@apchem.nagoya-u.ac.jp (A. Satsuma).

0021-9517/$ – see front matter
doi:10.1016/j.jcat.2005.10.009

should clarify the essential factors for the design of selective oxidation catalysts.

The objective of this study is to clarify the involvements in the surface functional species on the selective oxidation of propane. Promoted $(VO)_2P_2O_7$ catalysts were investigated as model catalysts, because the active bulk phase for the selective oxidation of alkane is already known to be $(VO)_2P_2O_7$ [28,29]. Furthermore, it has already been proposed that the surface V=O species on $(VO)_2P_2O_7$ is responsible for oxidation of *n*-butane [30–33] and that the surface V=O species can be measured by the nitric oxide ammonia rectangular pulse (NARP) technique [32–34]. For the measurement of surface acid sites, we previously reported that dimethylpyridine temperature-programmed desorption (DMP-TPD) is applicable for measuring Brønsted and Lewis acid sites on metal oxide catalysts [35]. In this report, the involvements of these functional groups in the oxidation of propane are investigated.based on the measurement of surface V=O species, Brønsted acid sites, and Lewis acid sites on a series of promoted $(VO)_2P_2O_7$.

2. Experimental

2.1. Catalyst preparation

Pure and promoted $(VO)_2P_2O_7$ catalysts were prepared from an aqueous media as reported previously [32–34]. 85% H_3PO_4 (0.24 mol) and $NH_2OH{\cdot}HCl$ were dissolved in 200 ml of distilled water and stirred at 353 K. Then V_2O_5 (0.1 mol) was slowly added into the solution and evaporated at 423 K. After drying at 403 K for 12 h, the $VOHPO_4{\cdot}0.5H_2O$ thus obtained was boiled in distilled water for 10 min. As for pure $(VO)_2P_2O_7$ (abbreviated as VP hereinafter), the $VOHPO_4{\cdot}0.5H_2O$ was calcined at 823 K in flowing N_2 for 2.5 h. The promoted $(VO)_2P_2O_7$ catalysts were prepared by impregnating an aqueous solution containing additive elements $VOHPO_4{\cdot}0.5H_2O$ by the incipient wetness method. $Sb(CH_3COO)_3$, $Ti(C_2H_5O)_4$, $ZrOCl_2{\cdot}8H_2O$, $HfOCl_2{\cdot}8H_2O$, $Cu(CH_3COO)_2{\cdot}H_2O$, and $Ce(CH_3COO)_3{\cdot}H_2O$ were used as sources of additives. The atomic ratio of additive metal was $M(\text{additive})/V = 0.05$. The promoted $VOHPO_4{\cdot}0.5H_2O$ was calcined at 823 K in flowing N_2 for 2.5 h. The catalyst names were abbreviated with VP (for the promoter element), as shown in Table 1.

2.2. Characterizations

X-ray diffraction (XRD) analysis was done with a Rigaku RINT-1200 diffractometer with Cu$K\alpha$ radiation. Raman spectra were achieved on powders at room temperature using a JASCO NRS-100 spectrometer. The exciting line of a semiconductor laser source at 532 nm was focused using a 100× objective. The spectral resolution was about 3 cm^{-1}. Infrared (IR) spectra were measured with a JASCO FT/IR-300 equipped with a diffuse reflectance unit. As for the spectra of catalyst bulk, the samples were diluted with KBr, and the spectra were measured using a triglycine sulfate detector with the resolution of 4 cm^{-1}. IR spectra of adsorbed pyridine were measured using a JASCO FT/IR-620 equipped with a diffuse reflectance unit connected to a flow system [35]. After calcination at 823 K for 2 h in flowing dry He, pyridine was saturated in the flowing He and adsorbed on the sample at room temperature. After purging in flowing dry He at room temperature for 4 h, an absorption spectrum was measured with 100× accumulation and resolution of 2 cm^{-1} using a mercury cadmium telluride detector.

Dimethylpyridine temperature-programmed desorption (DMP-TPD) was performed as reported previously [35]. Both 2,6-dimethylpyridine (2,6-DMP) and 3,5-dimethylpyridine (3,5-DMP) were used as probe molecules. 100 mg of a sample was placed in a U-shaped tubular cell and preheated at 673 K for 2 h in a dehydrated helium flow of 150 $cm^3\,min^{-1}$. After cooling to 523 K, the sample was exposed to a stream of the probe molecule diluted in helium for 30 min. Then the sample was left in flowing helium at 523 K for 120 min to purge any excess and/or weakly held probe molecules. Finally, the TPD measurement was performed from 523 to 1073 K at a heating rate of 5 K min^{-1}. The desorbed probe was detected with a flame ionization detector (FID).

NARP measurements were carried out as reported previously [32,33]. After oxidation of catalyst (0.1 g) in flowing oxygen at 773 K for 30 min, the sample was cooled to a predetermined temperature (450–600 K). Then NO–NH_3 mixture ($NO/NH_3 = 1/4$) gas was injected as a rectangular pulse with a width of 60 s. The number of surface V=O species was determined according to the analysis of produced nitrogen profile as described previously [32,36].

Table 1
Surface area and amount of active sites on pure and promoted $(VO)_2P_2O_7$ catalysts

Catalyst	Surface area (m^2g^{-1})	Surface V=O species		Amount of acid sites		
		(10^{-6} mol g^{-1})	(10^{-6} mol m^{-2})	Total (10^{-6} mol m^{-2})	Brønsted acid (10^{-6} mol m^{-2})	Lewis acid (10^{-6} mol m^{-2})
VP	9.3	59.5	6.4	0.60	0.35	0.25
VP–Sb	12.1	47.2	3.9	0.62	0.08	0.54
VP–Ti	17.6	84.5	4.8	0.63	0.28	0.35
VP–Zr	18.7	71.1	3.8	0.72	0.34	0.37
VP–Hf	25.2	95.8	3.8	0.36	0.15	0.21
VP–Cu	12.6	52.9	4.2	0.34	0.17	0.17
VP–Ce	45.6	104.9	2.3	0.27	0.15	0.13

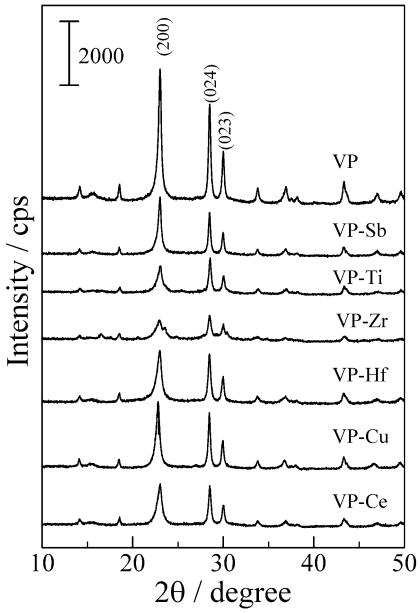

Fig. 1. XRD patterns of pure and promoted $(VO)_2P_2O_7$ catalysts.

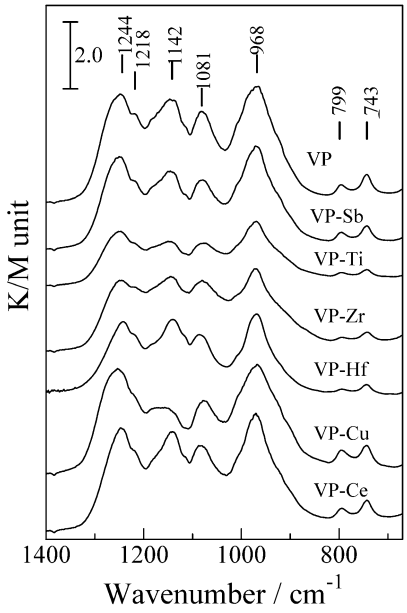

Fig. 2. IR spectra of pure and promoted $(VO)_2P_2O_7$ catalysts.

2.3. Propane oxidation

Selective oxidation of propane was carried out in a packed-bed reactor (Pyrex glass tube, 10 mm i.d., 12 mm o.d.). The reactor was heated in a fluidized sand bed. The catalyst weight was 2.0 g, and the same weight of quartz powder was added as a diluent. The flow rates of each component were C_3H_8, 2 $cm^3\,min^{-1}$; N_2, 36.5 $cm^3\,min^{-1}$; O_2, 9.8 $cm^3\,min^{-1}$; and steam, 14.1 $cm^3\,min^{-1}$. Gaseous products (propane, propene, CO, and CO_2) were analyzed by on-line gas chromatography. The products were separated with a Porapak Q column (2 m) and a MS-13X column (4 m) and analyzed by a thermal conductivity detector. Liquid products were trapped by ethanol at 273 K, separated with a Porapak QS (4 m) and PEG/celite (2.3 m), and detected by a FID. The catalytic activity on propane oxidation was measured after the confirmation of steady-state activity by treating in the reaction feed at 713 K for >8 h. A good carbon balance was observed (96–104%) for all of the experiments. Products included propene, acrylic acid, acetic acid, and COx (CO + CO_2).

Selective oxidation of propene was carried out by using the same apparatus and a catalyst spent in the oxidation of propane. The reaction conditions were as follows: 2.0 g of catalyst diluted with 2.0 g of quartz powder, flow rate of each component propene/N_2/O_2/steam = 2/36.5/9.8/14.1 $cm^3\,min^{-1}$, and reaction temperature 573–693 K. Acrylic acid, acetic acid, and COx (CO and CO_2) were detected as products.

3. Results

3.1. Bulk structure

Fig. 1 shows XRD patterns of pure and promoted VP catalysts. For all of the catalysts, only the patterns of the $(VO)_2P_2O_7$ phase [30,37–40] were observed; no other diffraction lines were observed. The addition of promoters resulted in a decrease in line intensity and line broadening of the (200) diffraction. The broadening of the (200) line of VP–Ti and VP–Zr was significant. Actually, the ratio of $I(200)/I(204)$ was originally 1.4 for pure VP, compared with 1.4 for VP–Sb; 1.2–1.0 for VP–Hf, –Cu, and –Ce; and 0.8 for VP–Zr and –Ti. Only in the case of VP–Cu was a small shift (0.005 nm) of the (200) diffraction line observed, indicating the formation of a solid solution of $(VO)_2P_2O_7$ with Cu.

Fig. 2 shows IR spectra of pure and promoted VP catalysts. The absorption bands at 743, 799, and 968 cm^{-1} can be assigned to stretching band of P–O–P, V–O=V, and V=O, respectively [39–41]. The bands attributable to PO_3 stretching mode were observed at 1081, 1142, 1218, and 1244 cm^{-1} [39–41]. Band intensity decreased slightly with the addition of promoters. The decreased intensity of the ν(V–O=V) band was particularly significant in the case of VP–Zr and VP–Ti, corresponding to the broadening of the (200) line in XRD patterns. In Raman spectra (figure not shown), only the bands characteristic of the $(VO)_2P_2O_7$ phase (i.e., ν(P–O–P) at 923 cm^{-1} and ν(V–O–P) at 1136 and 1182 cm^{-1} [42]) were observed. The bands of other phases, such as $VOPO_4$, were not observed. A decreased intensity of these bands after the addition of promoters was also observed, corresponding with the line broadening in the XRD patterns and the weakening of the IR bands.

3.2. Characterization of surface sites

As shown in Table 1, promoted VP catalysts had higher surface areas than pure VP catalyst. The number of surface V=O species increased with the addition of promoters, except for Sb and Cu. But the promoted VP catalysts exhibited lower surface concentrations of V=O species (i.e., the number of surface V=O species per surface area) than pure VP. Thus the increased number of surface V=O species is due to the increased surface

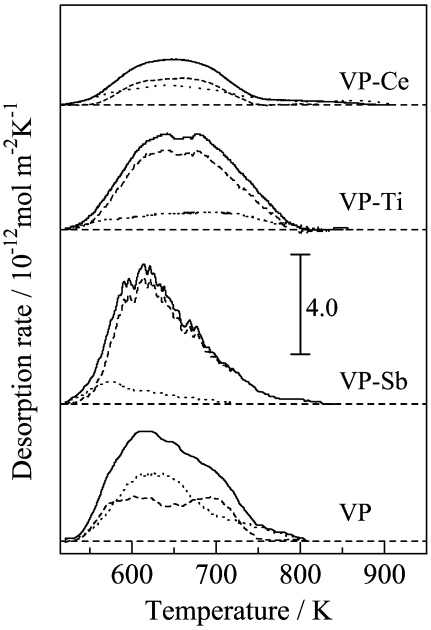

Fig. 3. Profiles of 3,5-DMP-TPD (solid line), 2,6-DMP-TPD (broken line), and difference profile of 3,5-DMP- and 2,6-DMP-TPD (dotted line) of pure and promoted $(VO)_2P_2O_7$ catalysts.

area, and the addition of promoters essentially decreased the surface concentration of V=O species on $(VO)_2P_2O_7$.

The amount and strength of surface Brønsted and Lewis acid sites were estimated using DMP-TPD by comparing the desorption profiles of 2,6-DMP and 3,5-DMP [35]. Fig. 3 shows examples of DMP-TPD profiles of pure and promoted VP catalysts. Because of steric hindrance of methyl groups adjacent to Lewis base of 2,6-DMP, 2,6-DMP selectively adsorbs on Brønsted acid sites. Thus, the profile of 2,6-DMP-TPD gives the strength distribution of Brønsted acid sites. In contrast, 3,5-DMP nonselectively adsorbs on both Brønsted and Lewis acid sites, and the difference profile denotes the distribution and amount of Lewis acid sites. As shown in Fig. 3, the 3,5-DMP-TPD profile of pure VP showed a broad single peak terminated at ca. 800 K, whereas the profile of 2,6-DMP-TPD was weighted around 700 K. The difference in these TPD profiles indicates that the Lewis acid sites are distributed mainly in weaker regions. But the 2,6-DMP-TPD profile of VP–Sb was significantly smaller, representing an abundance of Lewis acid sites on the VP–Sb catalyst. As for VP–Ti, TPD profiles also showed more Lewis acid sites than Brønsted acid sites. The amounts of Brønsted and Lewis acid sites were almost equivalent on the VP–Ce catalyst.

The numbers of Brønsted and Lewis acid sites thus measured are summarized in Table 1. The number of total acid sites for pure VP catalyst was 0.6×10^{-6} mol m^{-2}, whereas that for promoted catalysts was $0.27–0.72 \times 10^{-6}$ mol m^{-2}. These values are far lower than the theoretical surface concentration of cationic sites; for example, the theoretical surface concentration of V and P is 16.8×10^{-6} mol m^{-2} on the (100) basal plane [37]. This is because of the high purging temperature (573 K) in the TPD experiment for removal of physically adsorbed DMPs and for the selective adsorption of 2,6-DMP on Brønsted acid sites [35]. The addition of Sb, Ti, and Zr increased the number of Lewis acid sites, whereas the addition of Cu, Ce, and Hf decreased the number of Lewis acid sites. The amount of Brønsted acid sites decreased with the addition of these promoters.

Fig. 4 shows IR spectra of adsorbed pyridine on VP and VP–Sb catalysts. In the case of VP (Fig. 4a), the bands of adsorbed pyridine were observed at 1448, 1488, 1539, 1608, and 1637 cm^{-1}. The band of 1539 cm^{-1} is assignable to 8b mode of pyridinium ion adsorbed on Brønsted acid sites. Furthermore, a negative band was seen at 3660 cm^{-1} assignable to stretching vibration of surface OH group, although the signal-to-noise ratio was very low in this region (data not shown). This finding indicates that pyridine adsorbed on the acidic-surface OH group. The band of 1448 cm^{-1} is assignable to the 19b mode of coordinately held pyridine [43]. Because the band at 1448 cm^{-1} remained after the evacuation at 423 K, this band can be assigned to coordinately held pyridine adsorbed on Lewis acid sites. Other absorption bands can be assigned as follows: 1637 cm^{-1} to the 8a mode of pyridine on Brønsted acid sites, 1608 cm^{-1} to the 8b mode of pyridine on Lewis acid sites,

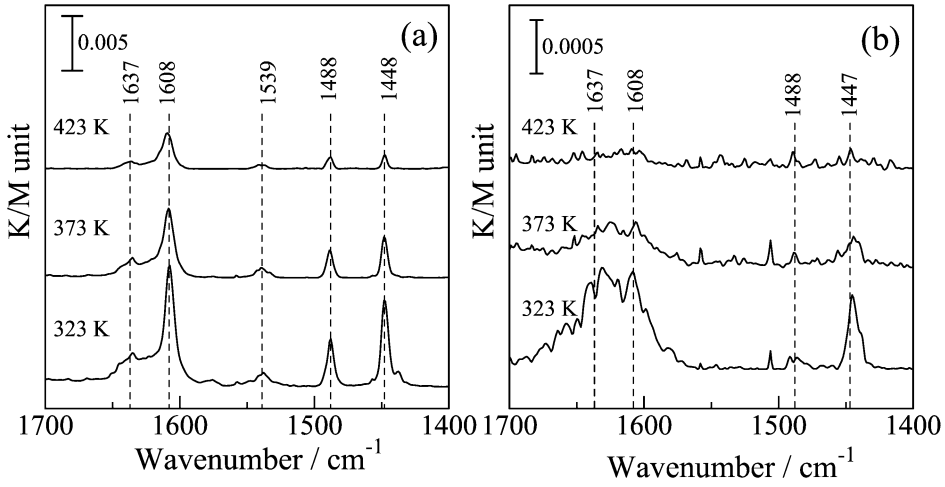

Fig. 4. IR spectra of adsorbed pyridine on (a) VP and (b) VP–Sb evacuated at various temperatures.

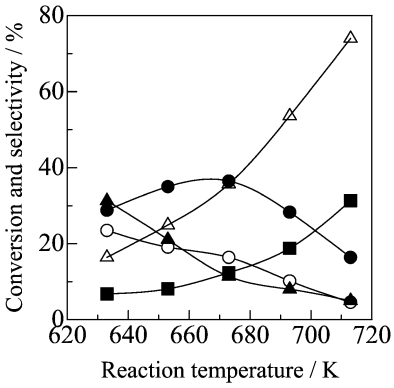

Fig. 5. Conversion of propane (closed square), selectivity of propene (closed triangle), acrylic acid (closed circle), acetic acid (open circle), and COx ($CO + CO_2$, open triangle) over pure VP catalyst as a function of reaction temperature.

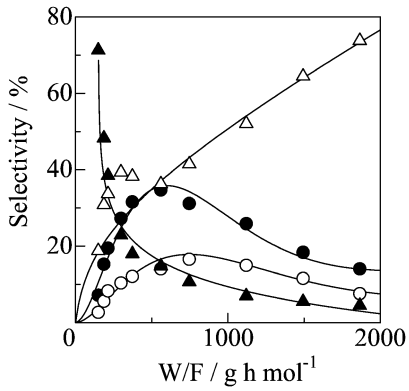

Fig. 6. Selectivities of products over pure VP catalyst at 653 K as a function of W/F. For the symbols, see Fig. 5.

and 1488 cm^{-1} to the 19a mode of pyridine on both sites. The spectra show that both Brønsted and Lewis acid sites are on pure VP surfaces.

In the case of VP–Sb (Fig. 4b), the band around 1540 cm^{-1} assignable to the 8b mode of the pyridinium ion adsorbed on Brønsted acid sites was not observed even at 323 K. Less-intense pyridine absorption bands are due to lower diffuse reflection of the sample. Although the signal-to-noise ratio was low, there was no change in the OH stretching region (data not shown). On the other hand, the band at 1447 cm^{-1} assigned to coordinately held pyridine on Lewis acid sites was clearly observed. These IR spectra were in a good accordance with the DMP-TPD profiles; that is, both Brønsted and Lewis acid sites present on pure VP catalyst, with Lewis acid sites abundant on VP–Sb.

3.3. Oxidation of propane

Fig. 5 shows the temperature dependence of propane conversion and selectivity over VP catalyst. Conversion of propane monotonously increased with increasing reaction temperature. The selectivity to acrylic acid first increased with temperature, achieved the maximum (37%) at 693 K, and then decreased with increasing reaction temperature. The selectivity to propene decreased, whereas that of COx increased with increasing reaction temperature. The maximum yield of acrylic acid was 6.2% at 693 K.

Fig. 6 shows product selectivities over pure VP catalyst as a function of W/F, that is, (catalyst weight)/(total flow rate). Propene selectivity monotonously decreased with W/F, suggesting consecutive reaction of propene to more oxidized products. Acrylic acid and acetic acid increased with W/F, reached a maximum at ca. $W/F = 560$–750 g h mol^{-1}, and then decreased with further increases in W/F. The selectivity to COx monotonously increased with increasing W/F. These patterns of selectivity clearly indicate the consecutive reaction of propane to propene, then to acrylic acid or acetic acid, and finally to COx. Because the induction period for the formation of COx is not clear, the contribution of direct pathway from propane to COx cannot be neglected. So far, several reaction schemes of propane oxidation have been proposed, as reviewed by Lin [6]. Over Mo–V–Te–Nb and Mo–V–Sb–Nb catalysts, direct oxidation from propane to 2-propanol, acetone, or 1-propanal has been proposed as a minor pathway [6,44,45], whereas Ai reported that only the oxidative dehydrogenation of propane to propene is the first step over V_2O_5–P_2O_5-based catalyst [17]. Propane oxidation goes through propane to propene, followed by parallel reactions to acrylic acid via acrolein and acetic acid via 2-propanol and acetone over Te-promoted V_2O_5–P_2O_5 catalyst. Our present result, shown in Fig. 6, agrees well with Ai's report, although the formation of acrolein, 2-propanol, and acetone was not observed. Therefore, from the present results, the reaction pathways of propane oxidation over $(VO)_2P_2O_7$ can be depicted as shown in Scheme 1. The contributions of active sites are discussed in Sections 4.2 and 4.3.

Activity and selectivity in propane oxidation over pure and promoted VP catalysts were compared. Fig. 7 shows the temperature dependence of propane conversion over promoted and pure VP catalysts. Propane conversion was in the following or-

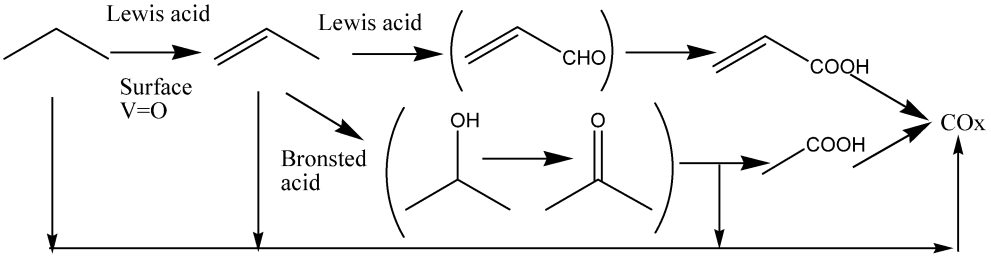

Scheme 1. Reaction scheme of selective oxidation of propane over $(VO)_2P_2O_7$.

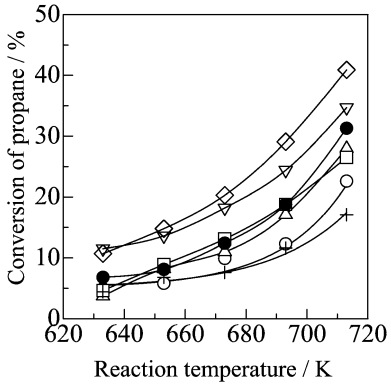

Fig. 7. Conversion of propane over VP (closed circle), VP–Sb (open circle), VP–Ti (open triangle), VP–Zr (open square), VP–Hf (open inverted triangle), VP–Cu (cross), and VP–Ce (diamond) as a function of reaction temperature.

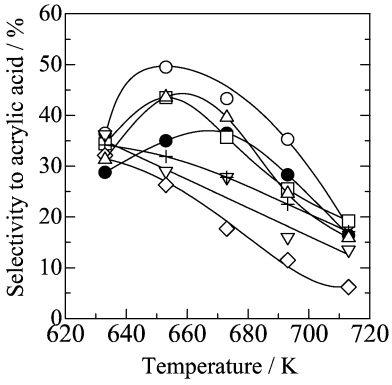

Fig. 8. Selectivity to acrylic acid as a function of reaction temperature. For the symbols, see Fig. 7.

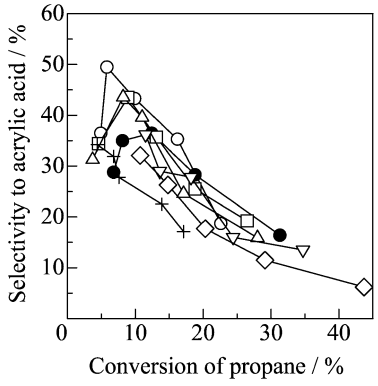

Fig. 9. Selectivity to acrylic acid in propane oxidation as a function of as propane conversion. For the symbols, see Fig. 7.

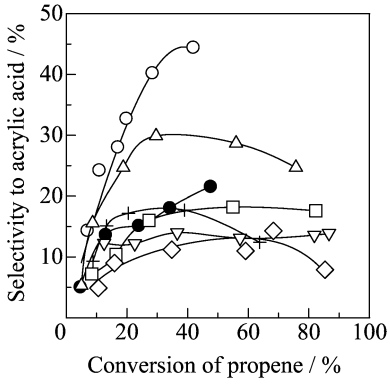

Fig. 10. Selectivity to acrylic acid in propene oxidation as a function of as propene conversion. For the symbols, see Fig. 7.

der: VP–Ce > VP–Hf > VP ∼ VP–Ti ∼ VP–Zr > VP–Sb > VP–Cu. Fig. 8 shows the selectivity to acrylic acid on various VP catalysts as a function of reaction temperature. Clearly, the selectivity to acrylic acid significantly increased from the addition of Sb, Ti, and Zr and decreased from the addition of Cu, Ce, and Hf. The maximum selectivities were observed at 653–673 K. The decreased selectivity at higher temperatures may be due to the consecutive oxidation of acrylic acid to COx. Fig. 9 plots the selectivity to acrylic acid at various temperatures as a function of propane conversion. Although the difference in selectivity to acrylic acid is smaller at the higher conversion level, a promotion effect on selectivity was clearly found at the lower conversion level; that is, the addition of Sb, Zr, and Ti improved selectivity, whereas the addition of Hf, Cu, and Ce suppressed it.

3.4. Oxidation of propene

As shown in Fig. 6 and Scheme 1, the oxidation of propane proceeds via oxidative dehydrogenation of propane to propene, followed by the consecutive reaction to acrylic acid or acetic acid and finally to COx. To clarify the role of the initial step of oxidative dehydrogenation and consecutive oxidation of propene, the oxidation of propene was performed over the same catalysts. The conversions of propene were higher than those of propane. The sequence of the activity was VP–Ce ∼ VP–Ti ∼ VP–Hf > VP–Zr > VP–Cu > VP > VP–Sb, which differs slightly from that of propane. Fig. 10 shows the selectivity to acrylic acid as a faction of propene conversion. At the conversion level of 20–30%, the selectivity to acrylic acid was in the order VP–Sb > VP–Ti > VP–Cu ∼ VP–Zr ∼ VP > VP–Hf > VP–Ce, almost the same as that in propane oxidation. The same trend in the selectivity to acrylic acid on oxidation of propane and propene suggests that the selectivity to acrylic acid in propane oxidation is determined mainly in the propene oxidation step.

4. Discussion

4.1. Bulk and surface structure of promoted $(VO)_2P_2O_7$

From the results of XRD patterns, IR spectra, and Raman spectra, it was confirmed that the catalysts examined in this study are composed of $(VO)_2P_2O_7$ phase with no other detectable phases. A slight modification of bulk structure was suggested for all of the promoted catalysts, that is, decreasing the crystallinity of $(VO)_2P_2O_7$ phase by adding promoters, which is more significant in VP–Zr and VP–Ti. In the case of VP–Cu, formation of solid solution was suggested. Although some modifications of bulk structure were detected, the catalysts prepared in this study are basically composed of $(VO)_2P_2O_7$ phase.

It is suggested that the surface V=O species on $(VO)_2P_2O_7$ act as active sites for the selective oxidation of *n*-butane

[30–33]. As shown in Table 1, the surface concentration of V=O species of VP catalyst was 6.4×10^{-6} mol m^{-2}. The measured value was higher than the theoretical concentration of surface V=O species on the (100) plane of $(VO)_2P_2O_7$ (4.2×10^{-6} mol m^{-2}) [37]. This result indicates that portions of V–O–V pair sites, which are originally in *trans* form, are rearranged to *cis* form on the actual real catalyst surface, as described previously [46]. As for the promoted catalysts, the surface concentrations of V=O species were lower than those of pure VP, $<4.8 \times 10^{-6}$ mol m^{-2}. Because there were only minor modifications of $(VO)_2P_2O_7$ phase, the decrease of the surface V=O species may be due mainly to substitution of vanadium sites with additive elements or poisoning of V=O species by small particles of additive oxides.

The surface concentration of acid sites was 0.6×10^{-6} mol m^{-2} on pure VP catalyst. Because the theoretical surface concentration of cationic sites is 16.8×10^{-6} mol m^{-2} on the (100) plane of $(VO)_2P_2O_7$, the actual concentration of acid sites was far lower than the theoretical concentration. This may be due to the high adsorption temperature of DMPs. The DMP-TPD experiment was carried out above 523 K, because of the low vapor pressure of DMPs, for the elimination of physically adsorbed DMP and for the selective adsorption of 2,6-DMP on Brønsted acid sites. These DMP-TPD profiles may reflect only the distribution of strong acid sites. Considering that the stronger acid sites should be more effective for the catalytic reactions, however, the acid sites measured by DMP-TPD can reflect the acid profiles that are critical of catalytic performance.

The presence of Brønsted and Lewis acid sites was also evaluated by IR spectra of adsorbed pyridine. The presence of both Brønsted and Lewis acid sites on VP was confirmed, whereas only the bands due to adsorbed pyridine on Lewis acid sites were observed on VP–Sb. In the case of VP, the ratio of integrated intensity of the bands at 1539 cm^{-1} (Brønsted acid) and 1448 cm^{-1} (Lewis acid) at 423 K was $I_{1539}/I_{1448} = 1.2/1$. Taking the relative extinction coefficient of these bands of around 1.0 into account [43], the ratio of Brønsted/Lewis acid sites estimated from IR of adsorbed pyridine is close to that from DMP-TPD, that is, (Brønsted acid)/(Lewis acid) $= 0.35/0.25 = 1.4/1$. As for VP–Sb, only the bands attributable to Lewis acid sites were observed, indicating Lewis acid sites are abundant on the surface of VP–Sb. This is also in good accordance in DMP-TPD. Only very low numbers of Brønsted acid sites (0.13×10^{-6} mol m^{-2}) were detected in 2,6-DMP-TPD of VP–Sb.

The effect of the promoters on catalyst structure was observed in the surface acid sites of $(VO)_2P_2O_7$. DMP-TPD profiles showed that the number of Lewis acid sites significantly increased from the addition of Sb, Ti, and Zr. This indicates that there is a synergistic effect on the electrostatic state of surface sites. Based on the concept proposed by Tanaka of using the electronegativity of the element defined by Pauling [47,48], the sequence of the electronegativity of additive ions is in the following order: Sb^{4+} (17.1) > Ti^{4+} (13.5) > Zr^{4+} (12.6) > Hf^{4+} (11.7) > Ce^{4+} (9.9) > Cu^{2+} (9.5). This order is in good agreement with the increase in Lewis acid sites on $(VO)_2P_2O_7$, suggesting that the higher electronegativity of additives may stabilize the Lewis acidity on surface unsaturated vanadium ions.

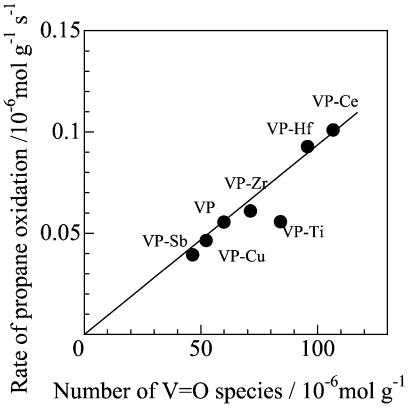

Fig. 11. Correlation between number of surface V=O species and reaction rate of propane at 653 K.

4.2. Controlling factor for activity

Higher propane conversion was obtained in the VP catalysts having higher surface area, such as Ce- and Hf-doped catalysts (Fig. 7; Table 1). However, the increase in propane conversion on VP–Ce was less than twice of pure VP, whereas VP–Ce showed 4.9 times greater surface area, indicating that these promoted catalysts had a lower reaction rate of propane per surface area. Comparing the propane conversion with the number of surface V=O species revealed that propane conversion increased in accordance with the number of surface V=O species per catalyst weight. Fig. 11 shows the reaction rate of propane as a function of the number of surface V=O species. Clearly, a linear correlation was observed between the oxidation activity and the V=O species, indicating that the surface V=O species is the determining factor for the oxidation activity of promoted $(VO)_2P_2O_7$. This finding is very reasonable, because the surface V=O species is suggested to be the active species of $(VO)_2P_2O_7$ for the selective oxidation of *n*-butane [30–33]. Fig. 11 also shows that the turnover frequency of surface V=O species is constant despite the addition of promoters examined in this study. Because a substantial amount of energy is required to selectively activate the methylene C–H bond of light alkanes [28,45,49], the oxidative dehydrogenation of propane to propene is thought to be the rate-determining step in the selective oxidation of propane. Actually, the reaction rates of propane (2.4–6.5 nmol m^{-2} s^{-1} at 653 K) were lower than that of propene (5.7–11.5 nmol m^{-2} s^{-1} at 633 K) for all of the catalysts. The strong dependence of propane conversion on the number of surface V=O species represents the contribution of surface V=O species to the initial oxidative dehydrogenation of propane to propene.

One may wonder whether Lewis acid sites are also possible factors for selective oxidation. Busca et al. [49] proposed that the key role of surface Lewis acid sites of $(VO)_2P_2O_7$ on light alkane oxidation is the abstraction of hydrogen from methylene C–H bond. In the present data, the reaction rate of propane could not be closely correlated with the Lewis

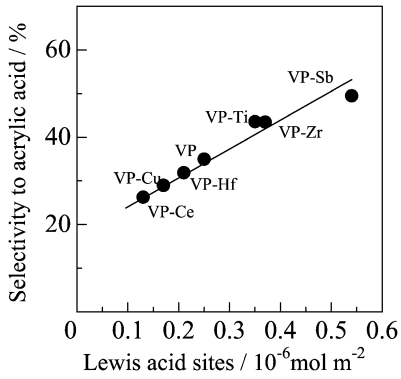

Fig. 12. Correlation between surface concentration of Lewis acid sites and selectivity to acrylic acid on propane oxidation at 653 K.

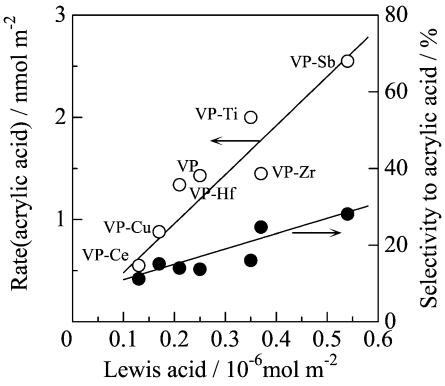

Fig. 13. Production rate and selectivity to acrylic acid on propene oxidation at 633 K as a function of surface concentration of Lewis acid sites.

acid sites; the order of the reaction rate of propane was VP (6.5 nmol m^{-2} s^{-1}) > VP–Hf (4.0) ∼ VP–Cu (4.0) > VP–Sb (3.6) ∼ VP–Ti (3.5) ∼ VP–Zr (3.5) > VP–Ce (2.4), whereas that of the surface concentration of Lewis acid sites was VP–Sb > VP–Ti ∼ VP–Zr > VP > VP–Hf > VP–Cu > VP–Ce (Table 1). However, the involvement of both Lewis acid sites and the surface V=O species in the oxidative dehydrogenation can be rationalized as follows. The first step in propane oxidation is the abstraction of hydrogen from propane, that is, cleavage of the methylene C–H bond by Lewis acid sites. After the abstraction of hydrogen, the abstracted hydrogen atoms are oxidized by lattice oxygen to form H_2O, and the reduced active sites are regenerated by gaseous O_2 [28,49]. The linear correlation between the number of surface V=O species and the reaction rate of propane can be rationalized by assuming that (1) the surface V=O species contribute to the formation of H_2O and regeneration of active sites and (2) the regeneration of the surface V=O species is the rate-determining process for turnover of the active sites.

4.3. Controlling factor for selectivity

The order of the maximum selectivity to acrylic acid was VP–Sb > VP–Ti ∼ VP–Zr > VP > VP–Hf > VP–Cu ∼ VP–Ce. Comparing the selectivity with the measured value of active sites shown in Table 1, this order was the same as that of surface concentration of Lewis acid sites. The surface concentration of Brønsted acid showed a quite different trend: VP ∼ VP–Zr > VP–Ti > VP–Cu ∼ VP–Hf ∼ VP–Ce > VP–Sb. Actually, as shown in Fig. 12, a good correlation was observed between the surface concentration of Lewis acid sites and the selectivity to acrylic acid. One may wonder whether the strength of Lewis acid sites should be taken into account, because the *x*-axis in the figure includes rather weak Lewis acid sites. As shown in Fig. 3, however, the distribution of Lewis acid sites is generally more weighted at higher temperatures than that of Brønsted acid sites. The DMP-TPD profiles indicate that VP–Sb and VP–Ti have stronger Lewis acid sites than pure VP. A similar correlation was also observed between the selectivity to acrylic acid and the surface concentration of stronger Lewis acid sites, which was observed above 650 K in DMP-TPD profiles. Therefore, it is clear that Lewis acid sites are the essential factor for the selective oxidation of propane to acrylic acid. In contrast, the selectivity of acetic acid was correlated with the surface concentration of Brønsted acid sites. Brønsted acid sites may play a role of catalytic cracking of C–C bond of surface intermediates derived from 2-propanol or acetone.

Fig. 13 shows the selectivity and formation rate of acrylic acid in the oxidation of propene as a function of the surface concentration of Lewis acid sites. In the oxidation of propene, acrylic acid production was also strongly dependent on the surface concentration of Lewis acid sites. Therefore, the selectivity in propane oxidation is determined mainly in the oxidation step of propene. The possible explanation for the key role of Lewis acid sites in propane oxidation is that surface Lewis acid sites may stabilize well-known allylic surface complexes, leading to the selective formation of acrylic acid via acrolein.

5. Conclusion

Selective oxidation of propane was performed over $(VO)_2P_2O_7$ promoted by various additives (Sb, Ti, Zr, Hf, Cu, and Ce), and the involvement of active sites was investigated. The addition of the promoters significantly affected activity and selectivity. A linear correlation was observed between the reaction rate of propane and the number of surface V=O species of the catalysts. The key role of surface V=O species in the initial oxidative dehydrogenation of propane to propene was indicated. The addition of Sb, Ti, and Zr to $(VO)_2P_2O_7$ significantly enhanced the selectivity to acrylic acid, and an increase in the surface concentration of Lewis acid sites was also observed. For all of the catalysts, a good correlation was observed between the selectivity to acrylic acid and the surface concentration of surface Lewis acid sites. Comparing the structure–activity relationship in propane and propene oxidation indicated the key role of Lewis acid sites in the selective pathway from propene to acrylic acid.

Acknowledgments

This work was supported by a Grant-in-Aid from the Ministry of Education, Culture, Sports, Science, and Technology, Japan, and the New Energy and Industrial Technology Development Organization (NEDO).

References

[1] G. Cavani, F. Trifiro, Catal. Today 51 (1999) 561.
[2] T. Ushikubo, H. Nakamura, Y. Koyasu, S. Wajiki, US Patent 5,380,933 (1995).
[3] H. Watanabe, Y. Koyasu, Appl. Catal. A 194–195 (1999) 479.
[4] T. Ushikubo, Catal. Today 57 (2000) 331.
[5] M. Lin, M.W. Linsen, EP Patent 962,253,A2 (1999).
[6] M. Lin, Appl. Catal. A 207 (2001) 1.
[7] W. Ueda, K. Oshihara, Appl. Catal. A 200 (2000) 135.
[8] R.K. Grasselli, Top. Catal. 15 (2000) 93.
[9] P. Botella, J.M. Lopez Nieto, B. Solsona, A. Mifsud, F. Marquez, J. Catal. 209 (2002) 445.
[10] Y.C. Kim, W. Ueda, Y. Moro-oka, Appl. Catal. A 70 (1991) 175.
[11] M.M. Bettahar, G. Constentin, L. Sabary, Appl. Catal. A 145 (1996) 1.
[12] X. Zhang, H. Wan, W.-Z. Weng, X.-D. Yi, J. Mol. Catal. A 200 (2003) 291.
[13] N. Mizuno, M. Tateishi, M. Iwamoto, Appl. Catal. A 128 (1995) 165.
[14] N. Mizuno, W. Han, T. Kudo, J. Catal. 178 (1998) 391.
[15] W. Li, W. Ueda, Catal. Lett. 46 (1997) 261.
[16] W. Li, K. Oshihara, W. Ueda, Appl. Catal. A 182 (1999) 357.
[17] M. Ai, J. Catal. 101 (1986) 389.
[18] Y.F. Han, H.M. Wang, H. Cheng, J.F. Deng, Chem. Commun. (1999) 521.
[19] J.K. Novakova, E.G. Derouane, Catal. Today 81 (2003) 247.
[20] G. Landi, L. Lisi, J.-C. Volta, Chem. Commun. (2003) 492.
[21] G. Landi, L. Lisi, J.-C. Volta, J. Mol. Catal. A 222 (2004) 175.
[22] H. Tsuji, Y. Koyasu, J. Am. Chem. Soc. 124 (2002) 5608.
[23] P. Botella, J.M. Lopez Nieto, B. Solsona, A. Mifsud, F. Marquez, J. Catal. 209 (2002) 445.
[24] Z. Zhao, X. Gao, I.E. Wachs, J. Phys. Chem. B 107 (2003) 6333.
[25] T. Katou, D. Vitry, W. Ueda, Chem. Lett. 32 (2003) 1028.
[26] J.N. Al-Saeedi, V.V. Guliants, O. Guerrero-Perez, M.A. Banares, J. Catal. 215 (2003) 108.
[27] J.M. Lopez Nieto, P. Botell, B. Solson, J.M. Oliver, Catal. Today 81 (2003) 87.
[28] G. Centi, F. Trifiro, J.R. Ebner, V.M. Franchetti, Chem. Rev. 88 (1988) 55.
[29] B.K. Hodnett, Heterogeneous Catalytic Oxidation, Wiley, Chichester, 2000.
[30] E. Bordes, Catal. Today 1 (1987) 499.
[31] G. Centi, F. Trifiro, G. Busca, J.R. Ebner, J.T. Gleaves, Proc. 9th Int. Congr. Catal. 4 (1988) 1538.
[32] D. Ye, A. Satsuma, A. Hattori, T. Hattori, Y. Murakami, Appl. Catal. 69 (1991) L1.
[33] D. Ye, A. Satsuma, A. Hattori, T. Hattori, Y. Murakami, Catal. Today 16 (1993) 113.
[34] A. Satsuma, Y. Tanaka, T. Hattori, Y. Murakami, Stud. Surf. Sci. Catal. 92 (1995) 281.
[35] A. Satsuma, Y. Kamiya, Y. Westi, T. Hattori, Appl. Catal. A 194–195 (2000) 253.
[36] A. Miyamoto, Y. Yamazaki, M. Inomata, Y. Murakami, J. Phys. Chem. 85 (1981) 2366.
[37] E. Bordes, P. Courtine, J.W. Johnson, J. Solid State Chem. 55 (1984) 270.
[38] F. Ben Abdelouahab, R. Olier, N. Guilhaume, F. Lefebvre, J.C. Volta, J. Catal. 134 (1992) 151.
[39] G. Busca, F. Cavani, G. Centi, F. Trifiro, J. Catal. 99 (1986) 400.
[40] M.L. Granados, J.C. Conesa, M. Fernandez-Garcia, J. Catal. 141 (1993) 671.
[41] Y. Kamiya, E. Nishikawa, T. Okuhara, T. Hattori, Appl. Catal. A 206 (2001) 103.
[42] Z. Xue, G.L. Scharader, J. Phys. Chem. B 103 (1999) 9459.
[43] H. Knozinger, Adv. Catal. 25 (1976) 184.
[44] E.K. Novakova, J.C. Vedrine, E.G. Derouane, J. Catal. 211 (2002) 226.
[45] E. Balcellis, F. Borgmeier, I. Grisstede, H.-G. Lintz, F. Rosowski, Appl. Catal. A 266 (2004) 211.
[46] A. Satsuma, Y. Tanaka, A. Hattori, T. Hattori, Y. Murakami, J. Chem. Soc., Chem. Commun. (1994) 1073.
[47] K. Tanaka, S. Ozaki, K. Tamaru, Syokubai (Catalysis) 6 (1964) 262.
[48] L. Pauling, Nature of Chemical Bond, third ed., Cornell Univ. Press, Ithaca, NY, 1960.
[49] G. Busca, G. Centi, F. Trifiro, Appl. Catal. 25 (1986) 265.